Hindawi
Advances in Civil Engineering
Volume 2021, Article ID 8847524, 15 pages
https://doi.org/10.1155/2021/8847524

Research Article

Intelligent Identification of Structural Damage Based on the Curvature Mode and Wavelet Analysis Theory

Longsheng Bao,[1] Yue Cao ,[1,2] and Xiaowei Zhang [1]

[1]*School of Transportation Engineering, Shenyang Jian Zhu University, Shenyang 110168, China*
[2]*College of Civil Engineering, Shenyang Jian Zhu University, Shenyang 110168, China*

Correspondence should be addressed to Yue Cao; 409439708@qq.com and Xiaowei Zhang; 76728552@qq.com

Received 10 August 2020; Revised 20 December 2020; Accepted 15 February 2021; Published 26 February 2021

Academic Editor: Leonidas Alexandros Kouris

Structural health monitoring is extensively used in new and old structures. During the process of monitoring, a large amount of data is generated. The selection of the appropriate methodology for the analysis of these data constitutes a major problem for maintenance personnel. Therefore, the purpose of this study is to programme data according to the curvature mode and wavelet transform theory to achieve automatic identification of structural damage and explore its applicability. First, the damage model is established with finite element software, and the applicability of the theory is verified by analysing the wavelet coefficients before and after structural damage. Thereafter, a programme is written to achieve the automatic output of the structural damage location based on the finite element results and basic theory. Data fitting is then performed to estimate the degree of structural damage. To evaluate the effects of the practical application of the programme, experimental verification is conducted. The experimental results demonstrate that the programme can automatically output the damage location and avoid the occurrence of calculation errors.

1. Introduction

Multiple damage areas emerge during the service period of a structure. These areas may be caused by improper maintenance or environmental influences. The occurrence of damage can reduce the local stiffness of the structure directly, and a considerable part of the damage is neither visible to the naked eye nor to visualisation instruments. If the problem is not detected, some hidden dangers to the structure will emerge over time that may potentially constitute a threat to people's properties and lives. Therefore, increasing attention has been paid to structural safety. Additionally, damage identification technology has developed rapidly in recent years. Some examples include the safety assessment of structures using techniques that range from traditional local nondestructive testing to global health monitoring [1, 2], as well as the development of techniques that span local ultrasonic testing to real-time acquisitions of the dynamic characteristic parameters with prearranged sensors. To achieve an overall damage assessment, many large bridges have been equipped with corresponding sensors for long-term health monitoring in recent years [3, 4]. In general, damage identification can be classified into theoretical research, laboratory verification, and structural health monitoring [5–10]. Most of the damage identification of actual structures relies on structural health monitoring. Whether the damage can be accurately identified depends on the correct analysis of the dynamic characteristic signals [11, 12]. Modern finite element software and the accuracy of various sensors are constantly improving, and signal processing technology is changing continually. Damage identification technology for damage responses based on structural health monitoring has gradually become a research focus at home and abroad [13, 14].

At present, the most popular damage identification methods include experimental modal analysis methods that combine system identification, vibration theory, vibration testing technology, signal acquisition and analysis, and other interdisciplinary techniques [15]. Typically, the dynamic characteristic parameters pertaining to structural damage include the natural frequency and the displacement and curvature modes [16]. A large amount of data has proved

that the curvature mode is more sensitive than damage indicators, such as the natural frequency [17, 18]. Additionally, the curvature mode is relatively easy to obtain and has good sensitivity; hence, it is the most cost-effective damage index [19, 20]. Tomaszewska [21] studied the relationship between the change in curvature mode and damage based on calculations. Dawari and Vesmawala and Dawari [22] performed similar calculations and obtained the curvature mode based on the difference operation of the displacement modes. Based on past and ongoing in-depth research studies, scholars have found that the perceived curvature mode has a poor recognition effect on the damage at the edges of the structure and when the structure has minor damage. Accordingly, it is necessary to develop a method to solve these problems.

In view of its "adaptability" and "mathematical characteristic"' [23], wavelet analysis has gradually revealed its advantages in signal processing technology. Wavelet transform relies on the wavelet's telescopic translation. This transform possesses several advantages and overcomes the shortcomings of the Fourier transform. It is an excellent mathematical tool for analysing non-steady-state signals. It has been extensively applied to various structures for damage identification [24–28]. Hou et al. used the Daubechies wavelet to transform the acceleration response of the structural dynamic model with wavelet transform and identified the loss position according to the sudden signal point changes [29, 30]. Pereira et al. studied a continuous wavelet transform (CWT) and applied it to the fault identification of gears connected to motors and generators to identify accurately the tooth on which the fault occurred [31].

Herein, structural damage identification technology is studied based on curvature mode normalization and wavelet transform theory. It is proved that the curvature mode data can be used as structural damage identification index data after the wavelet transform. The corresponding structural damage identification program is programmed in MATLAB and verified by finite element analysis and experimental measurements. Compared with the manual analysis and calculation, the program can automatically output the damage location and extent and yields a better recognition effect. It can also replace manual data analysis and processing to avoid the occurrence of calculation errors and other situations.

2. Basic Theory and Assumptions

2.1. Curvature Mode Theory. As a modal parameter, the curvature mode is a unique inherent deformation mode of the bending vibration of a bending structure. Because the curvature mode is the deformation mode of the neutral surface of the structure, it is relatively sensitive to local changes in the structure and can reflect changes in its local characteristics. Therefore, this theory is introduced into the damage identification of bending members.

When the beam is bent, the curvature of the neutral axis is calculated as follows:

$$\rho = \frac{M}{EI}, \tag{1}$$

where E is the elastic modulus of the material, I is the moment of inertia of the section, and M is the bending moment.

It can be inferred from equation (1) that the curvature of a certain point on the beam is inversely proportional to the corresponding structural stiffness; that is, the change in the stiffness of the structure can be reflected by the curvature [32].

Considering that the general structure service period is in the range of linear elasticity, from the point-of-view of material mechanics, the curvature of the component is

$$\rho = \frac{\delta''}{\left[1 + \left(\delta'\right)^2\right]^{3/2}}, \tag{2}$$

where δ is the displacement. In the case of small deformations, equation (2) can be transformed into

$$\rho = \delta''. \tag{3}$$

After introducing the definition of the curvature mode, ρ is the second derivative of δ, ρ is the curvature mode, and δ is the displacement formation.

In finite element analysis, the vibration modes obtained via modal analysis are generally displacement matrices, and the curvature modes can be easily obtained by calculating their variation laws using the central difference method.

In the actual structural health monitoring process, structural vibration conditions can be collected using preset global positioning system sensors and displacement sensors in cooperation with corresponding acquisition systems [33]. The maximum number of sensors should be deployed. The overall displacement matrix, δ, of the structure can be obtained via calculation based on the displacement, $\delta(x_i)$, of the measurement point on the bridge at a specific moment. The relevant expression is as follows [34]:

$$\delta = \left[\delta(x_1)\delta(x_2)\delta(x_3)\cdots\delta(x_i)\cdots\delta(x_{n-1})\delta(x_n)\right], \tag{4}$$

where i is the number of sensors.

When the actual sensor arrangement is sparse, the spline curve can be used for interpolation.

The curvature mode, $\rho(x_i)$, can be obtained using the central difference method of the displacement matrix as follows:

$$\rho(x_i) = \frac{\delta(x_{i-1}) - 2\delta(x_i) + \delta(x_{i+1})}{l_{i-1,i}, l_{i,i+1}}, \tag{5}$$

where $l_{i-1,i}$ is the distance from sensors $i-1$ to i and $l_{i,i+1}$ is the distance from sensors i to $i+1$.

The structural damage curvature mode can directly reflect the stiffness change during structural damage. If the damage to the structure is very small, the curvature mode can be normalised using the maximum normalisation method. Combined with the wavelet transform theory, the damage location and degree of damage of the structure become more prominent.

2.2. Wavelet Transform Theory. Once the structure is damaged, the local stiffness will decrease accordingly. Some characteristic parameters of the structure (such as displacement, modal formation, and modal curvature) will irregularly change or abruptly change following the damage. This sudden change contains a specific damage signal. These or other sudden changes usually correspond to the modulus maxima or zero-crossing points of the wavelet transform coefficients in the wavelet variation domain, and the degree of signal singularity corresponds to the change rule of the maximum scale of the wavelet transform coefficients. Chang and Chen [35] discussed the relationship between the wavelet transform modulus maximum (or zero-crossing) point and the signal point.

Suppose $\psi(x) \in L^2(R)$ $L^2(R)$ represents a square-integrable real number space, that is, a signal space with limited capabilities, and its Fourier transform is $\widehat{\psi}(\omega)$.

When function $\widehat{\psi}(\omega)$ satisfies the following admissibility condition,

$$C_\psi = \int_{-\infty}^{+\infty} \frac{|\widehat{\psi}(\omega)|^2}{|\omega|} d\omega \ < \infty, \tag{6}$$

then $\psi(x)$ is called a wavelet basis function, and the integral transformation can be defined as follows:

$$\left(W_\psi f\right)(a,b) = |a|^{-(1/2)} \int f(x) \overline{\psi\left(\frac{x-b}{a}\right)} d(x), \quad f(x) \in L^2(R). \tag{7}$$

In other words, the wavelet change of $(W_\psi f)(a,b)$ is based on $\psi(x)$, which is obtained after the expansion and contraction of scale a and the translation of b.

The aforementioned integral transformation to $f(x)$ is an integral CWT based on $\psi(x)$, wherein a is a scale factor that represents the expansion and contraction with frequency, and b is a time translation factor.

In simple terms, the process of CWT involves the calculation of the wavelet coefficients by getting as close as possible to the known signals based on the selected wavelet bases. The larger the obtained wavelet coefficient is, the greater the similarity between the wavelet base and the known signal. The signal can also be reconstructed according to the selected wavelet base and the wavelet coefficient.

Based on the above theory, the process of structural damage identification in this study is shown in Figure 1.

3. Results

3.1. Simulation Results and Wavelet Analysis. To establish a finite element analysis model for simply supported T-beams, the following parameters are set: beam length $L = 20$ m, elastic modulus $E = 32500$ MPa, density $\gamma = 2549$ kg/m^3, moment of inertia $I = 1.62 \times 10^{-1}$ m^4, and Poisson's ratio $\upsilon = 0.2$. The damage locations are distributed according to the working conditions and distributed at different sections for simulation. The degree of damage was simulated according to the damage and the stiffness of the section (estimated as the product of the modulus of elasticity and the moment of inertia of the section). In the simulation, the beam is first divided into 40 sections (as shown in Figure 2), the length of each section is 0.5 m, and the type of element is the beam element in the software Midas civil (2019). The constraint conditions are left-hinged and right sliding supports.

First, the structure is analysed to obtain the vibration modes of the damage-free model and the damage model for each node. Second, according to equation (5), the curvature mode is obtained and then normalised. Thereafter, the Daubechies 2 wavelet transform is selected in MATLAB (R2016b, MathWorks, Natick, MA, USA), and the damage-free model and wavelet coefficients are obtained. Finally, the above process is coded in MATLAB. In the general practical structural dynamic test process, low-frequency signals are easily collected accurately, and the high-frequency signal of the structure is not easily obtained accurately. Thus, the numerical simulation test used in this study uses the first-order mode of the structure in the analysis process. The structure's diagram is shown in Figure 2.

3.2. Damage Location Identification. To evaluate the applicability of this method and procedure in structural damage identification, three conditions were set up in this study for analyses. The specific working conditions are listed in Table 1.

After calculation, the frequency of the structure was obtained at different working conditions, which are presented in Table 2.

The set of damage levels in working condition 1 are 5%, 6%, 10%, 15%, and 20%. The damage location was set in section 9. The output single-damage wavelet coefficient difference diagrams based on the programme calculation are presented in Figures 3–7.

Figures 3–7 show that the position of the output damage is consistent with the preset damage position. Moreover, waveform analysis reveals that the waveform amplitude associated with the damaged area will be significantly increased as the degree of damage increases, and the amplitude of the undamaged position waveform is close to zero.

Working condition 2 constitutes the set of multidamage conditions with damage locations in sections 9, 19, and 34, and the damage degree is the same at the three locations. The five damage levels of 5%, 6%, 10%, 15%, and 20% are analysed. The output multidamage wavelet coefficient difference diagrams obtained through the programme calculation are presented in Figures 8–12.

It can be observed (from Figures 8–12) that when multiple points of damage of the same degree occur in the structure, an obvious waveform protrusion will occur at each damage level, and the output damage location will be consistent with the preset damage location. The extent of protrusion of the waveform will also increase as the degree of damage increases.

Working condition 3 is also a multidamage condition. It is a condition in which there are multiple points of damage of different degrees to the structure. In particular, 5% damage occurs in section 9, 6% damage occurs in section 19, and 10% damage occurs in section 34. The output

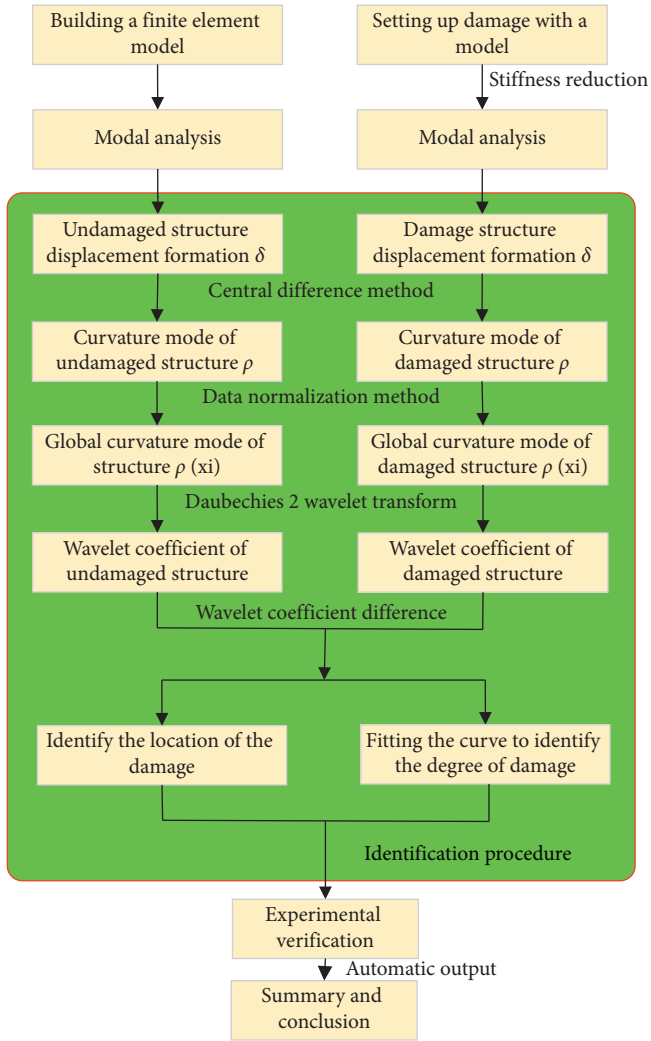

Figure 1: Flow chart of damage identification.

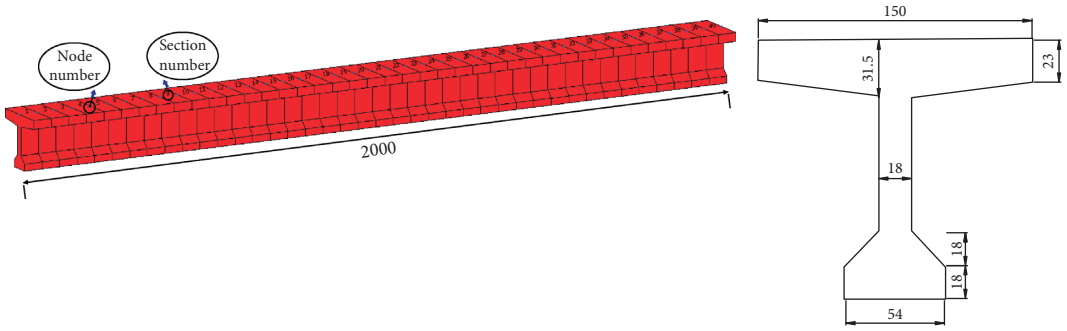

Figure 2: Structural layout of simply supported T-beam.

Table 1: List of working conditions used in the study.

Working condition	Damage location (m)	Section number	Degree of damage (%)
Working condition 1	4.25	9	5, 6, 10, 15, 20
Working condition 2	4.25, 9.25, 16.75	9, 19, 34	5, 6, 10, 15, 20
Working condition 3	4.25, 9.25, 16.75	9, 19, 34	5, 6, 10

Table 2: Frequency calculation values of each working condition (cycles/s).

Degree of damage (%)	Working condition		
	Working condition 1	Working condition 2	Working condition 3
5	6.560791	6.550404	
6	6.560071	6.547485	6.546205
10	6.557033	6.535200	
15	6.552837	6.518331	— —
20	6.548125	6.499508	— —

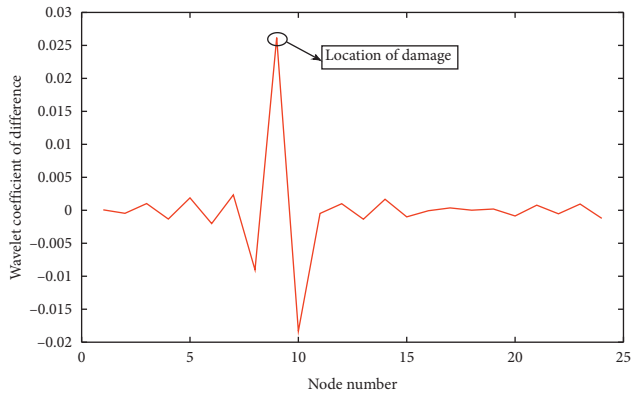

Figure 3: Wavelet coefficient difference graph for 5% damage in section 9.

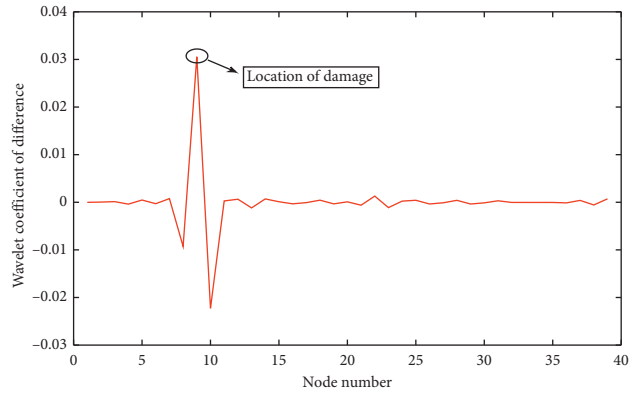

Figure 4: Wavelet coefficient difference graph for 6% damage in section 9.

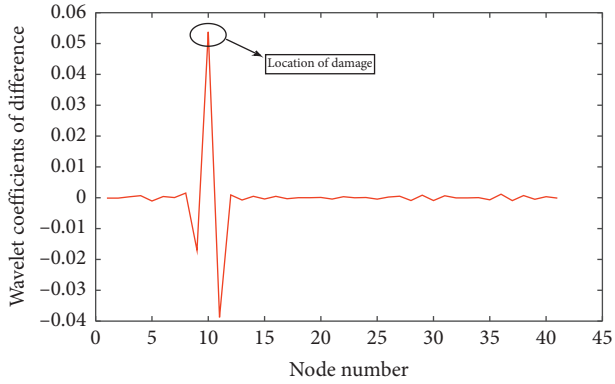

Figure 5: Wavelet coefficient difference graph for 10% damage in section 9.

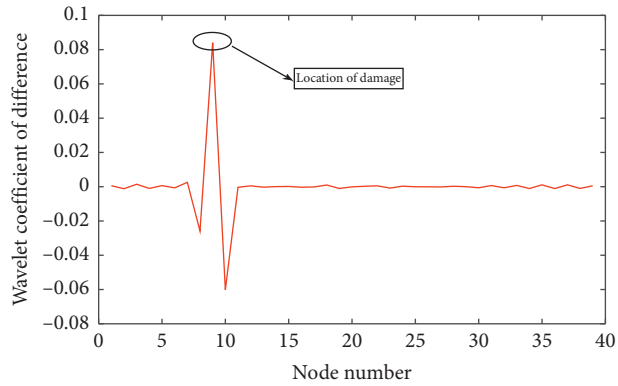

Figure 6: Wavelet coefficient difference graph for 15% damage in section 9.

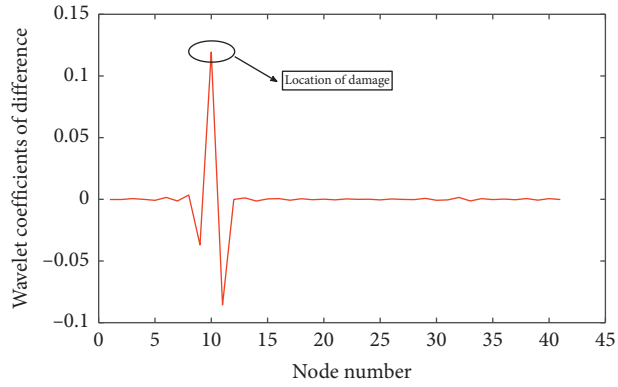

Figure 7: Wavelet coefficient difference graph for 20% damage in section 9.

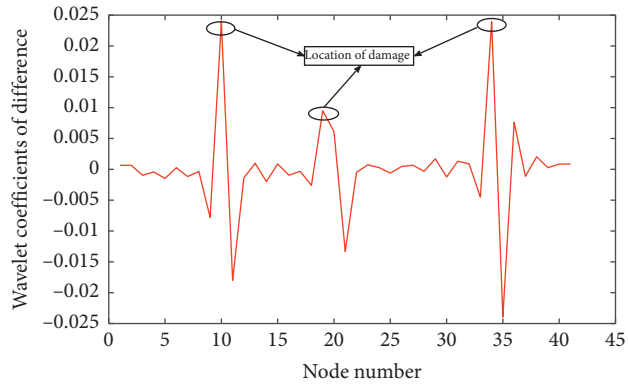

Figure 8: Wavelet coefficient difference for 5% damage in sections 9, 19, and 34.

multidamage wavelet coefficient difference diagrams obtained after programme calculation is presented in Figure 13.

As shown in Figure 13, when several degrees of structural damage occurs, the procedure can also accurately identify the location of the damage, and the effect of waveform recognition increases as the degree of damage becomes more profound.

Based on the above analysis, it can be observed that the programme can accurately output the location of the damage, regardless of whether single or multiple points of damage occur on the structure. Moreover, the recognition effect increases as the degree of damage becomes more profound.

3.3. Identification of Degree of Damage. The identification of the degree of structural damage is based on working condition 1, which has been discussed previously. A single-damage wavelet coefficient difference waveform is placed in the same coordinate system to generate a three-dimensional surface graph for analysis when the structural damage occurs at the levels of 5%, 6%, 10%, 15%, and 20%, as shown in Figure 14.

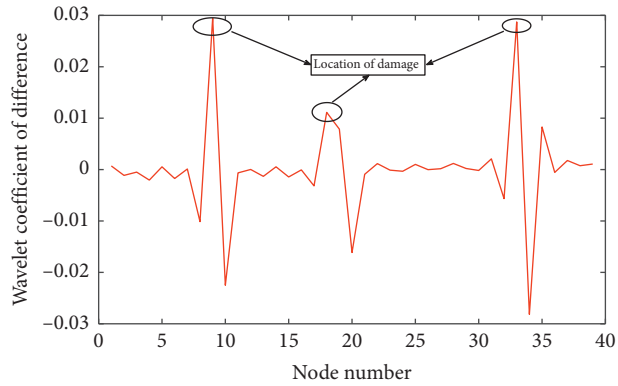

Figure 9: Wavelet coefficient difference for 6% damage in sections 9, 19, and 34.

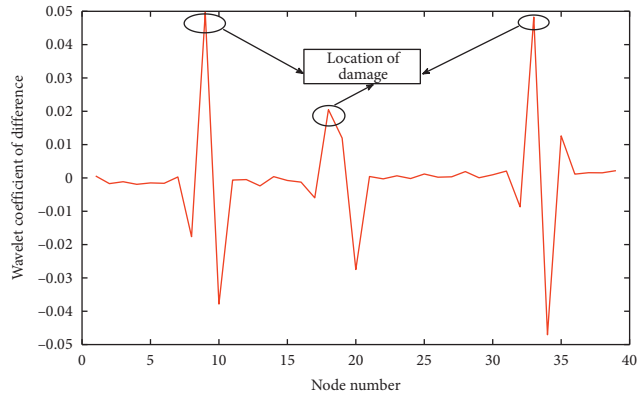

Figure 10: Wavelet coefficient difference for 10% damage in sections 9, 19, and 34.

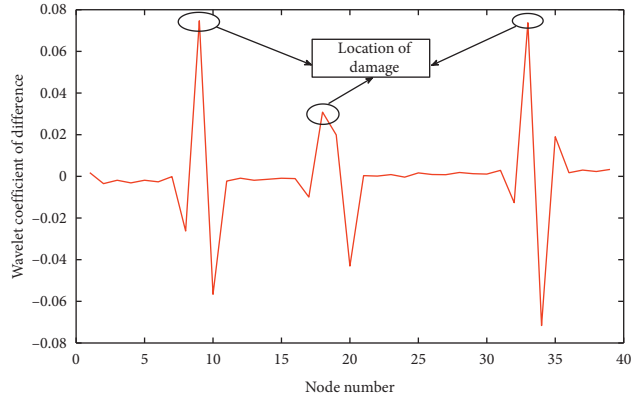

Figure 11: Wavelet coefficient difference for 15% damage in sections 9, 19, and 34.

It can be observed from Figure 14 that the peak at the damage point of the structure increases as the degree of damage increases. The programme's output peak point is then used to fit the curve, as shown in Figure 15.

From Figure 15, it can be observed that the curve fitting effect is very good, and the regression equation is formulated according to the following equation:

$$y = 1.965e - 06x^3 + 8.011e - 07x^2 + 0.005187x - 0.0004157, \quad (8)$$

where x is the peak of the wavelet coefficient difference. In other words, the degree of damage to the structure can be estimated according to the wavelet coefficient difference obtained by equation (8).

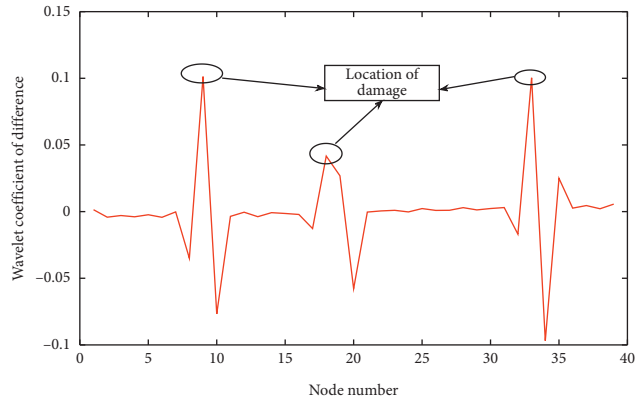

Figure 12: Wavelet coefficient difference for 20% damage in sections 9, 19, and 34.

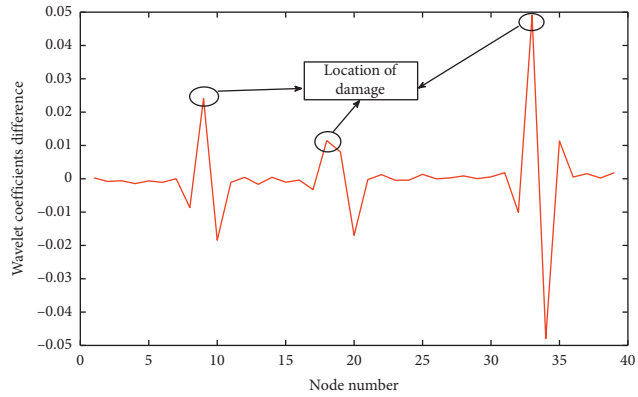

Figure 13: Wavelet coefficient differences of 5%, 6%, and 10% for damage in sections 9, 19, and 34, respectively.

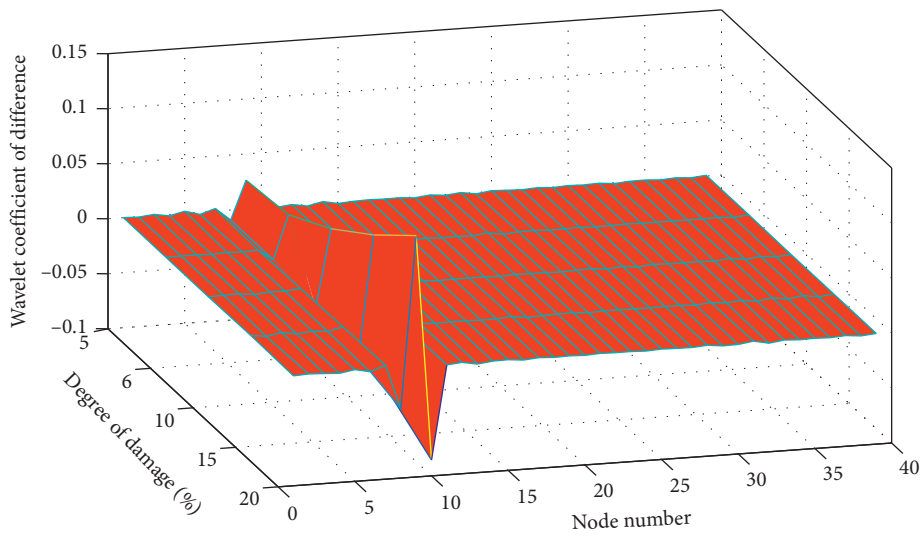

Figure 14: Three-dimensional curved surface of the single-damage wavelet coefficient in working condition 2.

When the structure has different degrees of damage in different sections, the five wavelet coefficient difference waveforms are placed in the same coordinate system to generate a three-dimensional surface map for analysis, as shown in Figure 16.

The output peak fitting curve is shown in Figure 17.

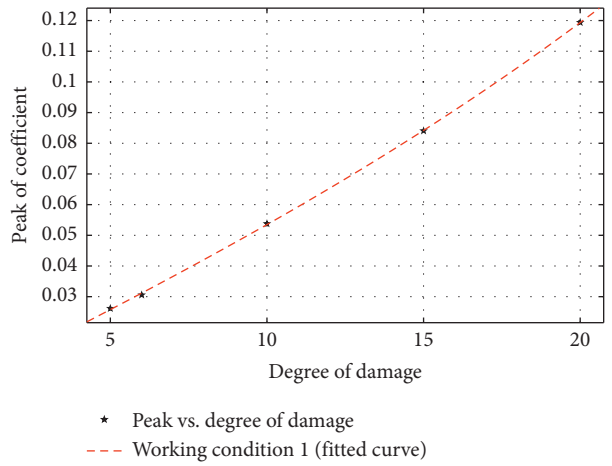

Figure 15: Fitting curve for structure with single damage.

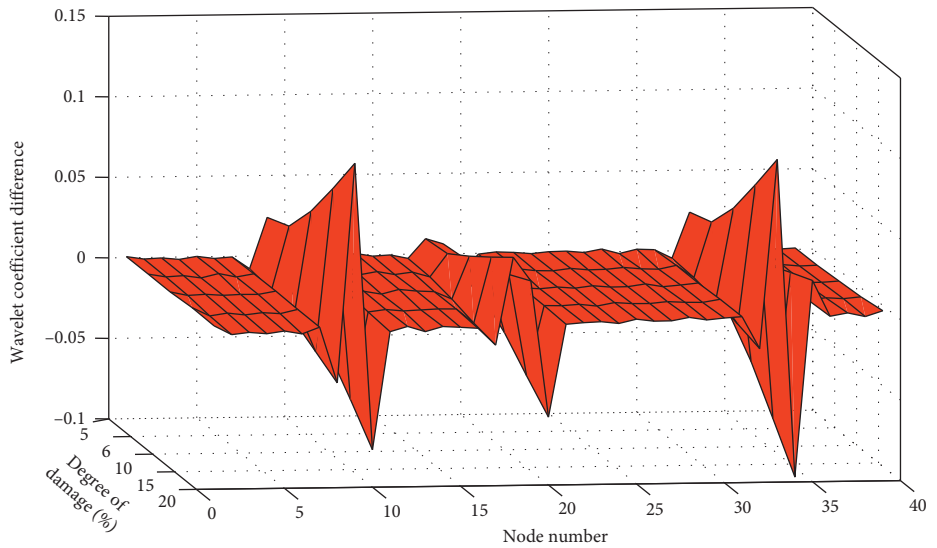

Figure 16: Three-dimensional surface of the wavelet coefficients of multiple points of damage in working condition 2.

As shown in Figure 17, the three curve fitting effects are still very good, and the regression equation can be obtained as shown in the following equation:

$$\begin{cases} y = 3.35 \times 10^{-4}x^3 - 0.0001167x^2 + 0.006311x - 0.005057, \\ y = 6.731 \times 10^{-5}x^3 - 2.884 \times 10^{-3}x^2 + 0.0023527x - 0.002761, \\ y = 7.816 \times 10^{-6}x^3 + 2.011 \times 10^{-3}x^2 + 0.004552x + 0.000659, \end{cases} \tag{9}$$

where y_1, y_2, y_3 denote the degrees of damages of the three damage points and x_1, x_2, x_3 are the peak values of the wavelet coefficient differences of the three damage points.

In other words, when there are multiple points of damage to the structure, the peak value of the wavelet coefficient difference obtained via the fitting formula and calculation can also be used to evaluate the degree of damage to the structure.

3.4. Experimental Verification. To verify the feasibility of the intelligent recognition programme further, six groups of I-shaped steel beams made of Q235 were set up. One group has a reference nondamaged steel beam, and five groups have damaged steel beams. Single and multiple damage are set to simulate the extent of damage by reducing the section size. The boundary condition is a hinged support condition on one side and sliding support on the other. The test was

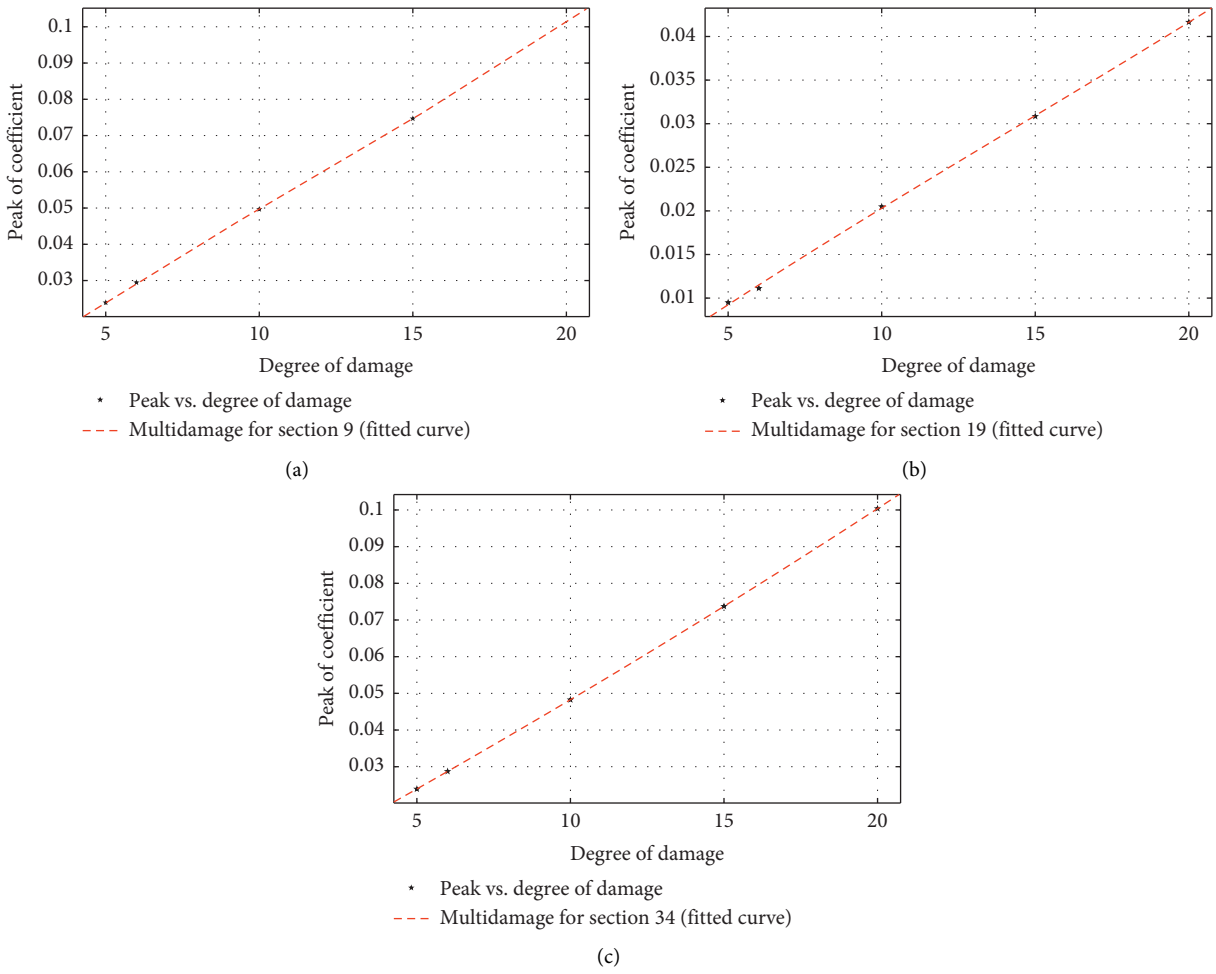

Figure 17: Fitted curves at multiple damage levels. Multidamage fittings for sections (a) 9, (b) 19, and (c) 34.

conducted using the force hammer multipoint excitation and the single-point response method. The acceleration sensor is arranged at the No. 4 node with a frequency response of 0.57000 Hz, an axial sensitivity of 100 mV/g, and a measurement range of ±50 g. Each parameter meets the data acquisition of the test beam. Before the beginning of data collection, the test beam was pretested, and the predivided joints of the I-shaped steel beams were knocked with a force hammer. Official acquisition begins after good data repeatability is achieved. Data from the same node are collected repeatedly, and the final data are obtained multiple times. The experimental field layout is shown in Figure 18.

The structural sketch and I-shaped steel beam cross-sections are shown in Figure 19. Affected by processing technology, the minimum degree of damage to the test beam is set at 5%. The parameters of the test beam are listed in Table 3.

Considering that the first-order frequency is easier to obtain in practical engineering applications, the first-order modal data are associated with the intelligent identification programme, and the output wavelet coefficient difference diagrams are presented in Figures 20–22.

Figures 21, 23, and 24 show that when single damage occurs to the structure, the waveform intensity at the damaged area will increase significantly. However, the waveform at the undamaged area also fluctuates to some extent, whereas the finite element calculation results are relatively flat. The programme can still output the same abscissa as the preset damage location. However, it will be difficult to identify the location of the structural damage if very minor damage occurs at other locations.

As shown in Figure 24, the location of the damage can be identified when there are multiple structural points of damage, but it is difficult to determine the degree of damage if these are similar. When minor damage occurs, the location of the damage cannot be determined; hence, the fitting effect of the damage degree is not good. However, when the structure size increases and the section partition density increases, the recognition effect will be improved considerably.

The fitting curves of experimental beams No. 2 to No. 5 are output by the programme, and the regression equation of the single-damage case is derived as shown in the following equation:

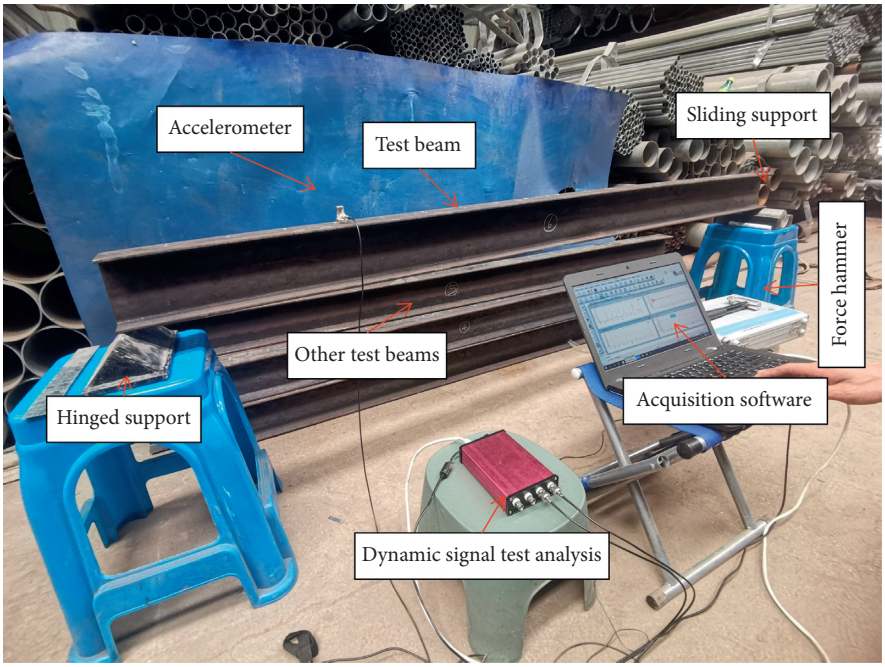

Figure 18: Experimental layout.

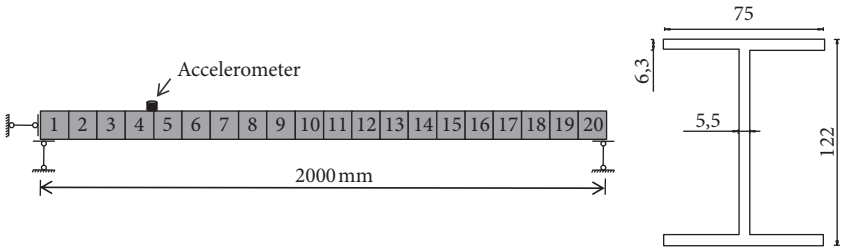

Figure 19: Diagrams of structure and cross section.

Table 3: List of working conditions.

Beam number	Damage location (mm)	Damage section	Degree of damage (%)
No. 1 beam	—	—	—
No. 2 beam	900–1000	10	5
No. 3 beam	900–1000	10	6
No. 4 beam	900–1000	10	10
No. 5 beam	900–1000	10	20
No. 6 beam	400–500, 900–1000, 1400–1500	5, 10, 15	5, 6, 10

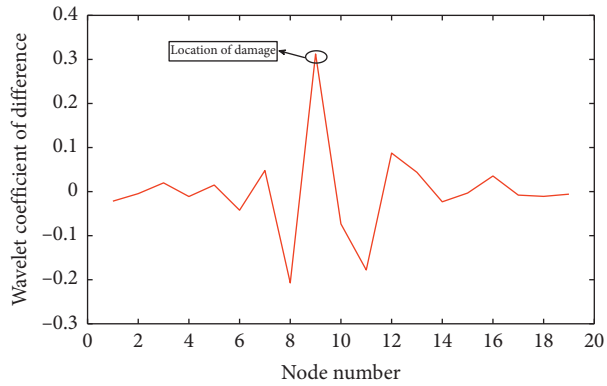

Figure 20: Wavelet coefficient difference for 10% damage in section 10.

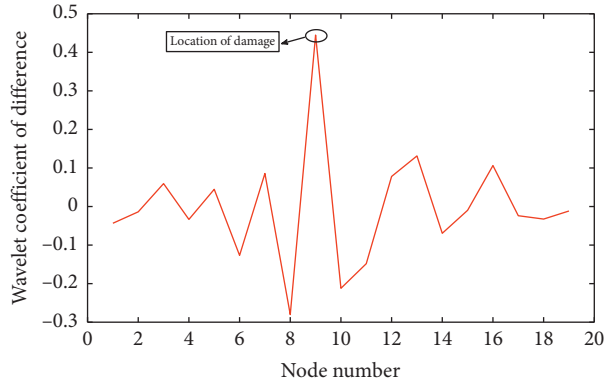

Figure 21: Wavelet coefficient difference for 20% damage in section 10.

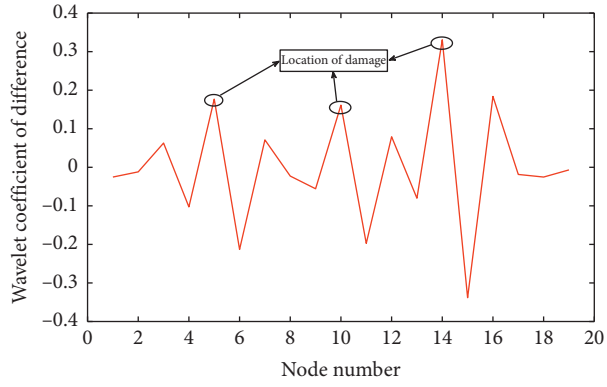

Figure 22: Wavelet coefficient difference for 20% damage in section 10.

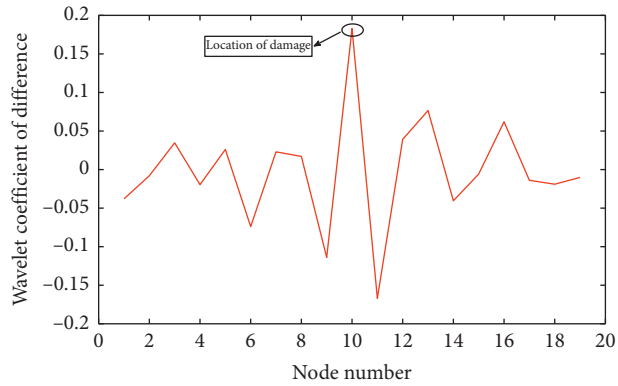

Figure 23: Wavelet coefficient difference for 5% damage in section 10.

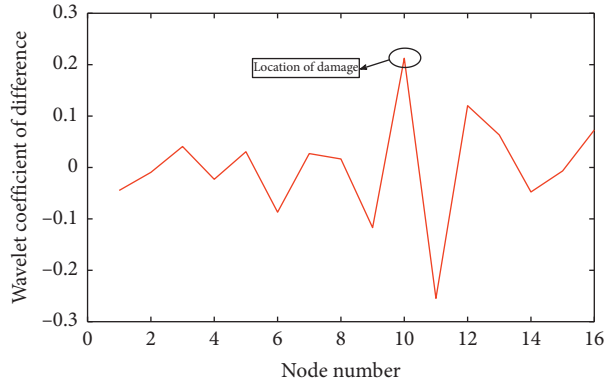

Figure 24: Wavelet coefficient difference for 6% damage in section 10.

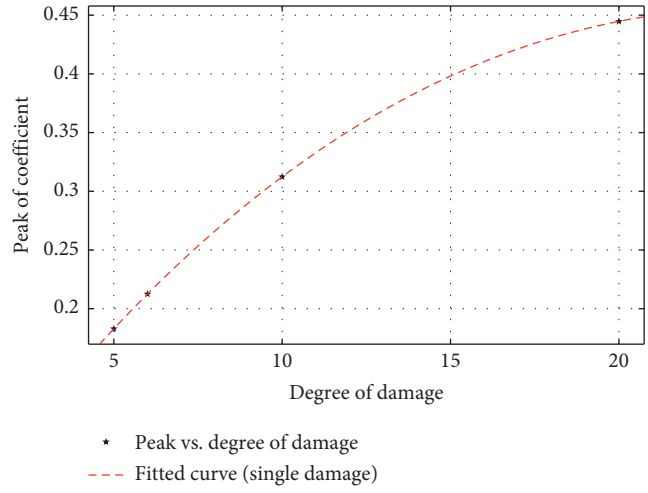

Figure 25: Fitted curve for single damage.

$$y = 6.064 \times 10^{-6}x^3 - 0.00105x^2 + 0.04068x + 0.005135. \quad (10)$$

As shown in Figure 25, the trend of the fitted curve of the test data is generally similar to that of the finite element simulation data, and the actual damage can also be evaluated by the peak value of the wavelet coefficient.

4. Conclusions

Based on the curvature mode and wavelet transform theory, this study used MATLAB to edit the structural damage intelligent identification programme and verified its feasibility based on numerical simulations and experimental data. The method proposed in this study has been used for

damage identification of simply supported beam systems. In the future, we will continue to study the application of this method in continuous beam systems or more complex bridge systems. The following are the conclusions we obtained:

(1) When single damage occurs in the structure, the small programme can accurately output the damage location, and the peak fitting formula of the wavelet coefficient difference can be used to estimate the degree of damage to the structure.

(2) When multiple points of damage occur in the structure, the programme can output the damage location. If multiple very small points of damage occur, this method may not be effective in identifying them. Considering that the stiffness of the structure usually decreases to some extent when the actual structure is damaged, this method is considered to be feasible.

(3) The vibration modes identified by the analysis system used in this test can be calculated as accurately as the last two decimal points. If the calculation accuracy can be improved further, the effect of damage identification will improve considerably. In addition, the components used in this experiment were small and had increased stiffness. If applied to the actual bridge structure, the experimental effect will be better. If the division accuracy of the structural sections is improved, it will also be helpful for the improvement of the effect of damage identification.

(4) The programme can be applied to bridge health monitoring systems in the future. It can read the vibration mode data in real-time and output the structural damage location in real-time. In this respect, the structural damage identification technology tends to be intelligent.

Data Availability

The data used to support the findings of this study were supplied by Longsheng Bao under license and so cannot be made freely available. Requests for access to these data should be made to Yue Cao.

Conflicts of Interest

The authors of this article confirm that the received funding that has been mentioned did not lead to any conflicts of interest regarding the publication of this manuscript.

Acknowledgments

The authors would like to thank Editage (http://www.editage.cn) for English language editing. This work was supported by the National Key R&D Program of China (2018YFC0809606 and 2018YFC0809600).

References

[1] B. D. Hedegaard, C. E. W. French, and C. K. Shield, "Time-dependent monitoring and modeling of I-35W St. Anthony falls bridge. I: analysis of monitoring date," *Journal of Bridge Engineering*, vol. 22, no. 7, Article ID 04017025, 2017.

[2] S. Yu and J. P. Ou, "Structural health monitoring and model updating of Aizhai suspension bridge," *Journal of Aerospace Engineering*, vol. 30, no. 2, Article ID B4016009, 2017.

[3] T. R. VanZwol, J. J. R. Cheng, and G. Tadros, "Long-term structural health monitoring of the crowchild trail bridge," *Canadian Journal of Civil Engineering*, vol. 35, no. 2, pp. 179–189, 2008.

[4] R. Zaurin, T. Khuc, and F. N. Catbas, "Hybrid sensor-camera monitoring for damage detection: case study of a real bridge," *Journal of Bridge Engineering*, vol. 21, no. 6, pp. 1–13, 2016.

[5] Y. Arici and K. M. Mosalam, "System identification of instrumented bridge systems," *Earthquake Engineering & Structural Dynamics*, vol. 32, no. 7, pp. 999–1020, 2003.

[6] G. Buda and S. Caddemi, "Identification of concentrated damages in euler-Bernoulli beams under static loads," *Journal of Engineering Mechanics*, vol. 133, no. 8, pp. 942–956, 2007.

[7] F. Ghrib, L. Li, and P. Wilbur, "Damage identification of Euler-Bernoulli beams using static responses," *Journal of Engineering Mechanics*, vol. 138, no. 5, pp. 405–415, 2012.

[8] E. M. Hernandez, "Identification of localized structural damage from highly incomplete modal information: theory and experiments," *Journal of Engineering Mechanics*, vol. 142, no. 2, pp. 1–9, 2015.

[9] M. Fraser, A. Elgamal, X. He, and J. P. Conte, "Sensor network for structural health monitoring of a highway bridge," *Journal of Computing in Civil Engineering*, vol. 24, no. 1, pp. 11–24, 2010.

[10] E.-T. Lee and H.-C. Eun, "Damage identification by the data expansion and substructuring methods," *Advances in Civil Engineering*, vol. 2018, Article ID 1867562, 12 pages, 2018.

[11] J. Li, H. Hao, and Z. W. Chen, "Damage identification and optimal sensor placement for structures under unknown traffic-induced vibrations," *Journal of Aerospace Engineering*, vol. 30, no. 2, Article ID B4015001, 2017.

[12] K. H. Hsieh, M. W. Halling, P. J. Barr, and M. J. Robinson, "Structural damage detection using dynamic properties determined from laboratory and field testing," *Journal of Performance of Constructed Facilities*, vol. 22, no. 4, pp. 238–244, 2008.

[13] K. K. Walsh, B. T. Kelly, and E. P. Steinberg, "Damage identification for prestressed adjacent box-beam bridges," *Advances in Civil Engineering*, vol. 2014, Article ID 540363, 16 pages, 2014.

[14] H. P. Zhu, J. Yu, and J. B. Zhang, "A summary review and advantages of vibration-based damage identification methods in structural health monitoring," *Engineering Mechanics*, vol. 28, no. 2, pp. 1–11, 2011.

[15] R. Yoshimoto, A. Mita, and K. Morita, "Parallel identification of structural damages using vibration modes and sensor characteristics," *Journal of Structural Engineering*, vol. 48, pp. 487–492, 2002.

[16] M. Georgioudakis and V. Plevris, "A combined modal correlation criterion for structural damage identification with noisy modal data," *Advances in Civil Engineering*, vol. 2018, Article ID 3183067, 20 pages, 2018.

[17] J.-T. Kim, Y.-S. Ryu, H.-M. Cho, and N. Stubbs, "Damage identification in beam-type structures: frequency-based method vs mode-shape-based method," *Engineering Structures*, vol. 25, no. 1, pp. 57–67, 2003.

[18] X. Zhang, "A connection between linear normal modes and lines of curvature on the potential surface," *Mechanics Research Communications*, vol. 34, no. 3, pp. 235–240, 2007.

[19] Y. Zhang, M. Kurata, and J. P. Lynch, "Long-term modal analysis of wireless structural monitoring data from a suspension bridge under varying environmental and operational conditions: system design and automated modal analysis," *Journal of Engineering Mechanics*, vol. 143, no. 4, Article ID 04016124, 2017.

[20] J. Chang, Y. H. Ren, and Z. H. Chen, "Experimental investigation of structural damage identification by combination index method under ambient excitation," *Engineering Mechanics*, vol. 7, pp. 130–135, 2011.

[21] A. Tomaszewska, "Influence of statistical errors on damage detection based on structural flexibility and mode shape curvature," *Computers & Structures*, vol. 88, no. 3-4, pp. 154–164, 2010.

[22] V. B. Dawari and G. R. Vesmawala, "Structural damage identification using modal curvature differences," *IOSR Journal of Mechanical and Civil Engineering*, vol. 4, pp. 33–38, 2013.

[23] M. Unser, "Wavelets: on the virtues and applications of the mathematical microscope," *Journal of Microscopy*, vol. 255, no. 3, pp. 123–127, 2014.

[24] Z. Jie, L. Zheng, and J. L. Chen, "Damage identification method based on continuous wavelet transform and mode shapes for composite laminates with cutouts," *Composite Structures*, vol. 191, pp. 12–23, 2018.

[25] L. H. Yam, Y. J. Yan, and J. S. Jiang, "Vibration-based damage detection for composite structures using wavelet transform and neural network identification," *Composite Structures*, vol. 60, no. 4, pp. 403–412, 2003.

[26] A. Gentile and A. Messina, "On the continuous wavelet transforms applied to discrete vibrational data for detecting open cracks in damaged beams," *International Journal of Solids and Structures*, vol. 40, no. 2, pp. 295–315, 2003.

[27] A. V. Ovanesova and L. E. Suárez, "Applications of wavelet transforms to damage detection in frame structures," *Engineering Structures*, vol. 26, no. 1, pp. 39–49, 2004.

[28] M. Rucka, "Damage detection in beams using wavelet transform on higher vibration modes," *Journal of Theoretical and Applied Mechanics*, vol. 49, no. 2, pp. 399–417, 2011.

[29] Z. Hou, M. Noori, and R. S. Amand, "Wavelet-based approach for structural damage detection," *Journal of Engineering Mechanics*, vol. 126, no. 7, pp. 677–683, 2000.

[30] S. Beskhyroun, T. Oshima, and S. Mikami, "Wavelet-based technique for structural damage detection," *Structural Control & Health Monitoring*, vol. 17, no. 5, pp. 473–494, 2010.

[31] A. L. V. Pereira, A. C. Gonçalves, R. Ribeiro, F. R. Chavarette, and R. Outa, "Detecting punctual damage to gears through the continuous Morlet wavelet transform," *Shock and Vibration*, vol. 2020, Article ID 8879565, 9 pages, 2020.

[32] A. L. Vidot-Vega and M. J. Kowalsky, "Relationship between strain, curvature, and drift in reinforced concrete moment frames in support of performance-based seismic design," *ACI Structural Journal*, vol. 107, no. 3, p. 291, 2010.

[33] M. J. Chae, H. S. Yoo, J. Y. Kim, and M. Y. Cho, "Development of a wireless sensor network system for suspension bridge health monitoring," *Automation in Construction*, vol. 21, pp. 237–252, 2012.

[34] A. Yalin and K. M. Khalid, "Statistical significance of modal parameters of bridge systems identified from strong motion data," *Earthquake Engineering & Structural Dynamics*, vol. 34, no. 10, pp. 1323–1341, 2005.

[35] C.-C. Chang and L.-W. Chen, "Damage detection of a rectangular plate by spatial wavelet based approach," *Applied Acoustics*, vol. 65, no. 8, pp. 819–832, 2004.